

Cite this: *J. Mater. Chem. C*, 2018, 6, 1224

## A large enhancement of magnetocaloric effect by chemical ordering in manganites†

Yanmei Wang,<sup>‡a</sup> Yinyan Zhu,<sup>‡a</sup> Hao Liu,<sup>a</sup> Hanxuan Lin,<sup>a</sup> Tian Miao,<sup>a</sup> Yang Yu,<sup>a</sup> Furong Han,<sup>b</sup> Wenbin Wang,<sup>a</sup> Jirong Sun,<sup>id</sup>\*<sup>b</sup> Lifeng Yin\*<sup>ac</sup> and Jian Shen<sup>id</sup>\*<sup>ac</sup>

For conventional ferromagnetic systems, the magnetocaloric effect (MCE) is dominated by the entropy changes upon magnetic phase transitions. For strongly correlated oxides such as manganites, in which competing magnetic orders coexist and respond to an external field differently, the MCE is more complex due to the electronic phase separation (EPS) phenomenon. Taking the well-known  $(\text{La}_{2/3}\text{Pr}_{1/3})_{5/8}\text{Ca}_{3/8}\text{MnO}_3$  (LPCMO) manganite as a model system, we investigated how the length scale of EPS phases affects the MCE. Specifically, the EPS length scale can be dramatically reduced by the spatial ordering of Pr dopants in the LPCMO system. Experimental results indicate that the magnetic entropy change of the Pr-ordered LPCMO is considerably larger than that of the Pr-random LPCMO by a factor up to six at the onset temperature of the ferromagnetic phase. A direct relation between the length scale of EPS and MCE has been established based on the experimental results.

Received 23rd November 2017,  
Accepted 2nd January 2018

DOI: 10.1039/c7tc05369j

rsc.li/materials-c

### Introduction

In recent years, the magnetocaloric effect (MCE)<sup>1</sup> has received considerable interest for refrigeration applications due to its high cooling capacity, low energy consumption and environmental friendliness.<sup>2</sup> For conventional ferromagnetic systems, the MCE is largely determined by entropy changes when a long-range spin order is formed.<sup>3–8</sup> For strongly correlated magnetic oxides, however, the MCE becomes more complex because the electronic phase separation (EPS) phenomenon is common in these materials, which feature the spatial coexistence of competing electronic phases in a wide range of temperatures.<sup>9–11</sup> Both magnetic and nonmagnetic phases may exhibit a large response to an external magnetic field and contribute to MCE. It is thus intriguing to study the MCE of strongly correlated oxides, especially those with pronounced EPS.

Colossal magnetoresistance (CMR) manganites are strongly correlated oxides in which EPS has been known to play a critical role in their metal–insulator transition and CMR behavior. Although the influence of EPS on the MCE has been studied

in previous work,<sup>12–26</sup> little effort has been made to control the MCE by manipulating EPS in manganites. In this work, we demonstrate how to influence the MCE by changing the length scale of EPS in manganites. The  $(\text{La}_{2/3}\text{Pr}_{1/3})_{5/8}\text{Ca}_{3/8}\text{MnO}_3$  system is chosen as the model system for two reasons. First, the LPCMO system exhibits strong EPS, with a coexisting anti-ferromagnetic insulating phase and a ferromagnetic metallic phase.<sup>27–31</sup> Second, the length scale of EPS in the LPCMO system can be controlled by spatially ordering Pr dopants<sup>32</sup> which has been achieved in the superlattices formed by alternatively growing a 2-unit-cell  $\text{La}_{5/8}\text{Ca}_{3/8}\text{MnO}_3$  (LCMO) layer and a 1-unit-cell  $\text{Pr}_{5/8}\text{Ca}_{3/8}\text{MnO}_3$  (PCMO) layer (ordered LPCMO or O-LPCMO). The phase domains have a considerably smaller size than those of the conventional LPCMO epitaxial thin films (random LPCMO or R-LPCMO) with the same thickness and nominal doping concentration. We found that for both systems the magnetic entropy change exhibits peaks at two temperatures that correspond to the onset (220 K) and percolation (60 K) of the ferromagnetic phase. The magnetic entropy change of O-LPCMO is consistently larger than that of R-LPCMO by a factor up to six at the onset temperature of the ferromagnetic phase. A direct relation between the length scale of EPS and MCE has been established based on our experimental results.

### Results and discussion

#### Effect of Pr ordering on EPS in the LPCMO system

The O-LPCMO type  $[(\text{LCMO})_2/(\text{PCMO})_1]_{53}$  superlattices and R-LPCMO films with the same thickness (60 nm) and the same

<sup>a</sup> State Key Laboratory of Surface Physics and Department of Physics, Fudan University, Shanghai 200433, China. E-mail: Shenj5494@fudan.edu.cn, lifengyin@fudan.edu.cn

<sup>b</sup> Beijing National Laboratory for Condensed Matter Physics and Institute of Physics, Chinese Academy of Sciences, Beijing 100190, China. E-mail: jrsun@iphy.ac.cn

<sup>c</sup> Collaborative Innovation Center of Advanced Microstructures, Nanjing 210093, China

† Electronic supplementary information (ESI) available. See DOI: 10.1039/c7tc05369j

‡ Yanmei Wang and Yinyan Zhu contributed equally to this work.

nominal doping concentration were grown on single crystal (100)-orientated SrTiO<sub>3</sub> substrates by pulsed laser deposition (laser wavelength = 248 nm, fluence = 2 J cm<sup>-2</sup>, and repetition rate = 2 Hz) at 800 °C, in an atmosphere of 8 × 10<sup>-4</sup> mbar oxygen pressure (8% ozone). The unit cell-by-unit cell growth was *in situ* monitored by intensity oscillations of reflection high-energy electron diffraction (RHEED). The films were then post annealed at 950 °C for 3 h in a flowing oxygen atmosphere to improve oxygen stoichiometry. The magnetic properties were measured using a Superconducting Quantum Interference Device (SQUID).

The length scale of EPS and the corresponding physical properties of the O-LPCMO and R-LPCMO films are dramatically different. Fig. 1(A and B) show typical magnetic force microscopy (MFM) images of the O-LPCMO and R-LPCMO films acquired at various temperatures. Statistical analysis indicates that the length scale of EPS in O-LPCMO is nearly 10 times smaller than that in R-LPCMO. The volume fraction of the ferromagnetic metallic (FMM) phase can be determined by initial magnetization curves measured using a SQUID. As shown in the inset of Fig. 1(C), the initial fast increase of magnetization is caused by the spin alignment of the FMM phase along the external field, and the FMM volume fraction can thus be determined by the ratio between the initial fast increasing magnetization and the saturation magnetization. The results are shown in Fig. 1(C), which clearly indicate that the volume fraction of the FMM phase in O-LPCMO is significantly higher than that in R-LPCMO. Fig. 1(D) shows the comparison of temperature-dependent magnetization for the O-LPCMO and R-LPCMO films. The calculated dM/dT curves in the inset show two distinct peaks at a high temperature and a low temperature, which correspond to the onset and percolation of the ferromagnetic phase, respectively. We note that the

observed differences between the O-LPCMO and the R-LPCMO films essentially reproduce our previous results. The underlying physical mechanism is closely tied to the spatial ordering of the Pr dopants as explained in our previous work.<sup>32</sup>

### MCE of O-LPCMO and R-LPCMO systems

Having known the differences between the physical properties and the EPS length scales of the O-LPCMO and the R-LPCMO films, we now study their influence on the MCE of these two systems. In general, the magnetic entropy change ( $\Delta S_{(H,T,P)}$ ) at a fixed temperature ( $T$ ), magnetic field ( $H$ ) and pressure ( $P$ ) can be calculated from a series of isothermal  $M-H$  curves using the following equation,<sup>33</sup>

$$\Delta S_{(H,T,P)} = S_{(H,T,P)} - S_{(H=0,T,P)} = \int_0^H \left( \frac{\partial M}{\partial T} \right)_{H,P} dH \quad (1)$$

where  $\partial M/\partial T$  is the first derivative of magnetization with respect to temperature. For the case of the LPCMO system, there exists a large thermal hysteresis for the temperature dependent magnetization curves below the charge ordering temperature ( $T_{CO}$ ). To minimize the thermal hysteresis effect, for each temperature, the  $M-H$  curves need to be measured using the following procedure. (1) The sample was cooled down to the preset temperature from room temperature (RT) under zero magnetic field. (2) At this temperature, the virgin  $M-H$  curve was first measured with an increasing magnetic field from 0 to 7 T, and then the field was reduced to zero for the second measurement of the  $M-H$  curve from 0 to 7 T. (3) The field is reduced to zero again and the sample was warmed up to RT, followed by a demagnetization operation to erase the remnant magnetization in the sample and the magnet. (4) Steps 1–3 were repeated for the next preset temperature. Fig. 2(A and B)

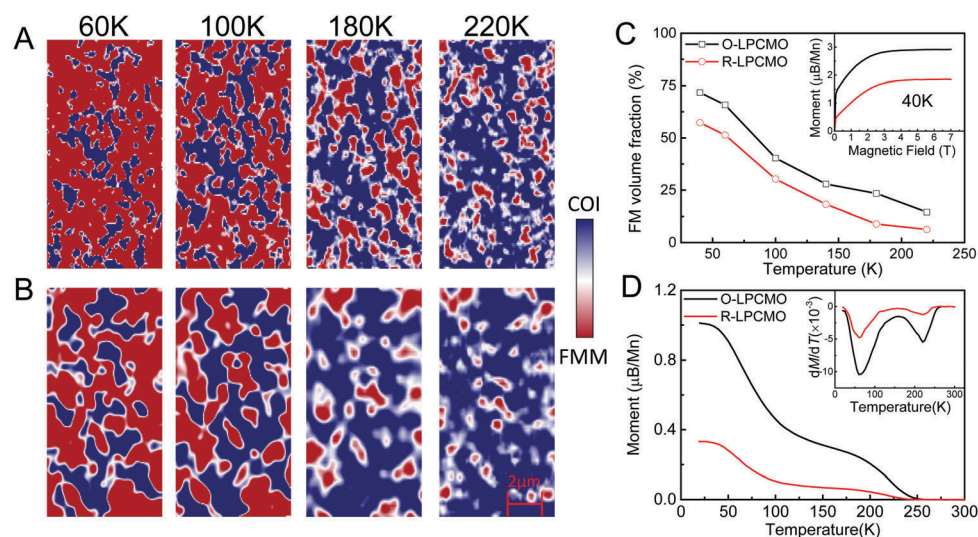


**Fig. 1** (A) and (B) Show typical magnetic force microscopy (MFM) images of the O-LPCMO and R-LPCMO films acquired at various temperatures under 1 T field cooling (the magnetic field was applied perpendicular to the sample surface), respectively. The scanning areas are 7 × 10 μm<sup>2</sup>. (C) The temperature-dependent FMM phase volume fraction for O-LPCMO and R-LPCMO films which is determined by initial magnetization curves measured using a SQUID (as shown in the inset). (D) The temperature-dependent magnetization for the O-LPCMO and R-LPCMO films. The inset is dM/dT curves.

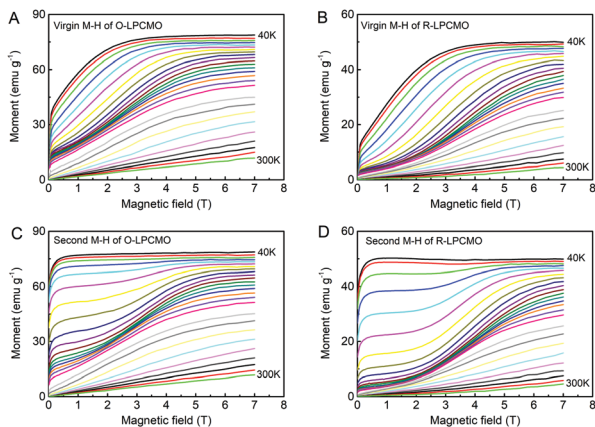


Fig. 2 (A and B) Virgin  $M-H$  curves of O-LPCMO and R-LPCMO, respectively. (C and D) Second  $M-H$  curves of O-LPCMO and R-LPCMO, respectively. The measurements were performed in the range of 40 K and 300 K with a 10 K interval.

show the virgin  $M-H$  curves measured at various temperatures between 40 K and 300 K with a 10 K interval for the O-LPCMO and R-LPCMO films, respectively. As mentioned above, the initial fast increase of magnetization reflects the response of the FMM phase to an external field, which shows that the volume fraction of the FMM phase in the O-LPCMO films is significantly higher than that in the R-LPCMO films. Fig. 2(C and D) show the corresponding second  $M-H$  curves of the O-LPCMO and the R-LPCMO films, respectively. The second  $M-H$  curves exhibit different characteristics from those of the virgin  $M-H$  curves, which reflect the reversibility of the field-induced COI to the FMM phase transition as will be discussed later.

Fig. 3 shows the temperature dependence of the calculated magnetic entropy change ( $-\Delta S$ ) for different magnetic fields using eqn (1). As expected, all  $-\Delta S(T)$  curves show two distinct peaks around  $T_{CO}$  and  $T_C$  corresponding to the onset of the FMM phase and percolation of the FMM phase, respectively. At low fields, the low temperature peak (LTP) near  $T_C$  is higher than the high temperature peak (HTP) near  $T_{CO}$  for both O-LPCMO and R-LPCMO films. With the increasing field, both

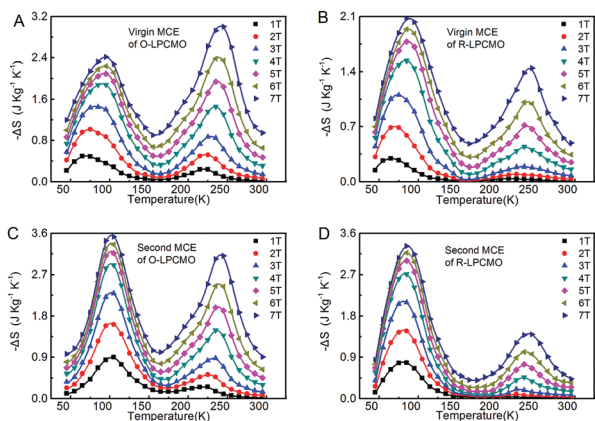


Fig. 3 Temperature-dependent magnetic entropy change ( $-\Delta S$ ) at different magnetic fields.

peaks increase noticeably in height and shift towards higher temperatures. Interestingly, for the O-LPCMO system, the HTP deduced from the virgin  $M-H$  curves grows more rapidly and becomes even higher than the corresponding LTP.

Fig. 4(A and B) show the field dependent height of the HTP and LTP deduced from the virgin and second  $M-H$  curves for O-LPCMO and R-LPCMO, respectively. The aforementioned field-induced crossover of the virgin HTP and LTP height occurs at  $\sim 5$  T for O-LPCMO. Such crossover does not occur for the R-LPCMO system and the LTP remains higher than the HTP up to the maximum applied field (7 T). For the second  $M-H$  process, the LTP values of both O-LPCMO and R-LPCMO increase significantly and stay higher than the HTP at all fields.

Fig. 4(C) shows the field dependence of the HTP and LTP height ratio of the O-LPCMO and R-LPCMO films. While the LTP values of the two types of films are comparable, the HTP values of the O-LPCMO films are considerably larger than those of the R-LPCMO films at all fields, reaching the maximum of about 6 times larger at around 1.5 T. With the increasing field, the difference between the O-LPCMO and the R-LPCMO films becomes smaller for both LTP and HTP values. Fig. 4(D) shows the field dependence of the positions of HTP and LTP for both O-LPCMO and R-LPCMO. The HTP positions are nearly the same for the O-LPCMO and the R-LPCMO films no matter if measured in virgin  $M-H$  or second  $M-H$  processes, and they all shift towards higher temperatures with increasing field. The LTP positions of the O-LPCMO films are at higher temperatures than those of the R-LPCMO films and exhibit a clear shift towards higher temperatures in the field range of 2–4 T during the virgin  $M-H$  process.

Because the LPCMO films exhibit pronounced EPS, the entropy changes with the field applied along the hard axis (surface normal) are worthy to be investigated as well. While the  $M-H$  curves measured along the hard axis (see ESI,† Fig. S1) are

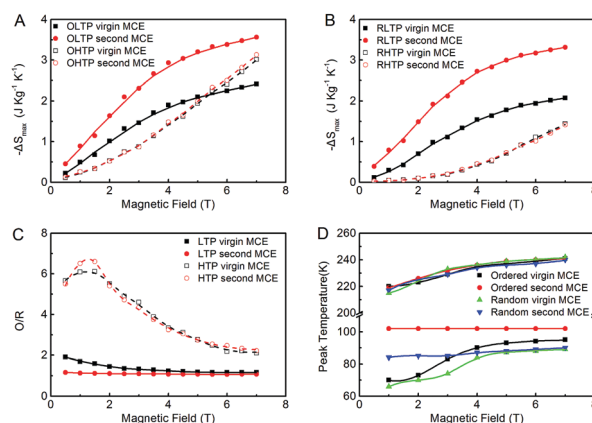


Fig. 4 (A and B) Show the field dependent height of the HTP and LTP deduced from the virgin and second  $M-H$  curves for O-LPCMO and R-LPCMO, respectively (OLTP stands for LTP of O-LPCMO, OHTP stands for HTP of O-LPCMO, RLTP stands for LTP of R-LPCMO, and RHTP stands for HTP of R-LPCMO). (C) The field dependent HTP and LTP height ratio between the O-LPCMO and R-LPCMO films. (D) The field dependent positions of the HTP and LTP for both the O-LPCMO and R-LPCMO films.

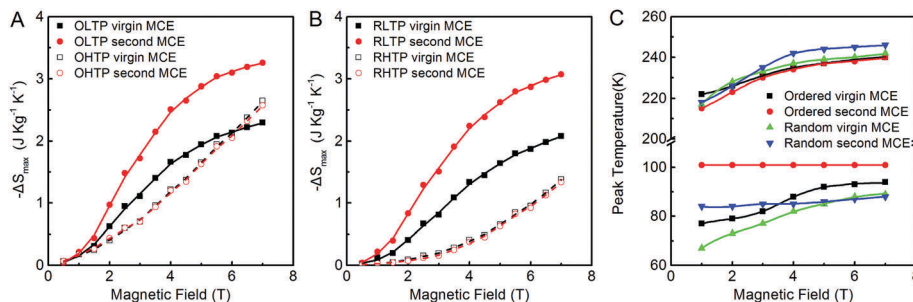


Fig. 5 (A and B) show the field dependent height of the HTP and LTP deduced from the virgin and second  $M-H$  curves (out-of-plane) for O-LPCMO and R-LPCMO, respectively. (C) The field dependent HTP and LTP height ratio of the O-LPCMO and R-LPCMO films.

different from those measured along the in-plane easy axis (Fig. 2), the calculated  $-\Delta S(T)$  curves along the out-of-plane hard axis (see ESI,† Fig. S2) are similar to those determined along the in-plane easy axis. Consequently, the field dependence of the HTP and LTP values and the positions measured along the hard axis (Fig. 5) exhibits a similar trend to those measured along the easy axis (Fig. 4).

## Discussion

We now turn to discuss the correlation between EPS and the observed common trend of the entropy changes in the LPCMO systems. The double peaks, *i.e.* HTP and LTP, reflect the onset of FMM domain formation and the percolation of the FMM domains, as shown in Fig. 1. With the increasing magnetic field, the COI phase starts to transform into the FMM phase and the FMM domains expand at the expense of COI domains leading to the general increase of HTP and LTP values in a wide field range for both O-LPCMO and R-LPCMO. In general, the LTP height increases faster in a low field, while the HTP height increases faster at a high field. This is understandable considering the fact that the transition from the COI phase to the FMM phase is relatively easier at low temperatures ( $T_C$ ) than at high temperatures ( $T_{CO}$ ), leading to a fast increase of the LTP (HTP) peak height at a lower (higher) field. It is also reasonable that the LTP determined from the second  $M-H$  curves has larger values than that determined from the virgin  $M-H$  curves, while the corresponding HTP values exhibit a slight difference. This is because the field-induced transition from the COI to the FMM phase is fully reversible at a high temperature ( $T_{CO}$ ), but becomes partially reversible, *i.e.* more ferromagnetic, at a low temperature ( $T_C$ ). The reversibility of the COI to FMM transition can also be used to explain the position change of the LTP and HTP, as shown in Fig. 4(D).

There are two major differences between O-LPCMO and R-LPCMO in their entropy changes. (1) The O-LPCMO system has larger HTP and LTP values than the R-LPCMO system at all fields, although the difference decreases with the increasing field. The difference is particularly great for the HTP peaks, reaching a factor of 6 at about 1.5 T field. (2) The HTP height of O-LPCMO increases quickly with the increasing field, and becomes even larger than the LTP height about 5 T during the virgin magnetization process. The HTP height remains

smaller than the LTP height for the R-LPCMO system up to the maximum field applied (7 T). These differences between O-LPCMO and R-LPCMO are caused by different EPS domain sizes and FMM volume fractions in the two systems. As shown in Fig. 1(C), the FMM volume fraction near  $T_{CO}$  (220 K) is 13% and 5% for O-LPCMO and R-LPCMO, respectively. Provided that the percolation limit of the FMM phase roughly follows the two-dimensional random percolation model ( $\sim 50\%$ ), both the O-LPCMO and the R-LPCMO films are significantly below the FMM percolation limit and require a large magnetic field to form the long range ferromagnetic order. Nevertheless, the O-LPCMO system has a higher FMM volume fraction and is thus closer to the percolation limit than the R-LPCMO system. Moreover, the EPS domains in the O-LPCMO system have a smaller size, which requires lower fields to be generated from the COI phase than R-LPCMO does. This explains why the HTP of O-LPCMO increases much faster with the increasing field than that of the R-LPCMO system. The situation becomes different at a lower temperature near  $T_C$ , at which the FMM volume fractions are 66% and 51% for O-LPCMO and R-LPCMO, respectively. Considering the fact that the entropy change gradually approaches the saturation level near the percolation limit, it is understandable why the difference between the LTP values of the two systems is small.

## Conclusions

In summary, we have directly compared the temperature and field dependence of the MCE of the O-LPCMO and the R-LPCMO systems. The O-LPCMO system exhibits considerably larger magnetic entropy changes at phase transition temperatures. We attribute the enlarged MCE of the O-LPCMO system to a smaller EPS length scale, which tends to exhibit a larger response to the external field due to the smaller energy barrier. Our observation indicates that in complex oxides such as manganites, the MCE is strongly affected by EPS and its response to an external field. The MCE becomes tunable if one can develop methods to control the characteristics of EPS. This opens a new pathway to extend the MCE in complex magnetic oxides for future applications.

## Conflicts of interest

There are no conflicts to declare.

## Acknowledgements

This work was supported by the National Key Research and Development Program of China (2016YFA0300701, 2016YFA0300702); the National Basic Research Program of China (973 Program) (2014CB921104); the National Natural Science Foundation of China (11504053); the Shanghai Municipal Natural Science Foundation (14JC140050000 and 17ZR1442600); and the China Postdoctoral Science Foundation (2016M601488 and 2017T100265).

## References

- 1 E. Warbug, *Ann. Phys.*, 1881, **249**, 141–164.
- 2 A. M. Tishin and Y. I. Spichkin, *The magnetocaloric effect and its applications*, CRC Press, 2016.
- 3 M. Balli, S. Jandl, P. Fournier and D. Dimitrov, *Appl. Phys. Lett.*, 2016, **108**, 102401.
- 4 X. Y. Tan, P. Chai, C. M. Thompson and M. Shatruk, *J. Am. Chem. Soc.*, 2013, **135**, 9553.
- 5 V. Franco, J. S. Blazquez, B. Ingale and A. Conde, *Annu. Rev. Mater. Res.*, 2012, **42**, 305–342.
- 6 M. Balli, S. Jandl, P. Fournier and M. M. Gospodinov, *Appl. Phys. Lett.*, 2014, **104**, 232402.
- 7 S. Gama, A. A. Coelho, A. de Campos, A. M. G. Carvalho, F. C. Gandra, P. J. von Ranke and N. A. de Oliveira, *Phys. Rev. Lett.*, 2004, **93**, 237202.
- 8 V. K. Pecharsky and K. A. Gschneidner Jr, *Phys. Rev. Lett.*, 1997, **78**, 4494.
- 9 C. N. R. Rao and B. Raveau, *Colossal magnetoresistance, charge ordering and related properties of manganese oxides*, World Scientific, 1998.
- 10 Y. Tokura, S.-W. Cheong and H. Y. Hwang, *Colossal Magnetoresistance Oxides, Monographs in Condensed Matter Science*, Gordon & Breach, New York, 1991.
- 11 Y. Tokura and Y. Tomioka, *J. Magn. Magn. Mater.*, 1999, **200**, 1.
- 12 A. Alberca, *et al.*, *Sci. Rep.*, 2015, **5**, 17926.
- 13 M. Anwar and B. H. Koo, *Electron. Mater. Lett.*, 2015, **11**, 614.
- 14 N. Bingham, P. Lampen, M. Phan, T. Hoang, H. Chinh, C. Zhang, S. Cheong and H. Srikanth, *Phys. Rev. B: Condens. Matter Mater. Phys.*, 2012, **86**, 064420.
- 15 A. Biswas, T. Samanta, S. Banerjee and I. Das, *Appl. Phys. Lett.*, 2008, **92**, 212502.
- 16 A. Dutta, N. Gayathri and R. Ranganathan, *Phys. Rev. B: Condens. Matter Mater. Phys.*, 2003, **68**, 054432.
- 17 M. Khondabi, H. Ahmadvand, P. Kameli, P. Amirzadeh, H. Salamati, P. Dasgupta and A. Poddar, *J. Appl. Phys.*, 2015, **118**, 233908.
- 18 A. Lima Sharma, P. Sharma, S. McCall, S.-B. Kim and S.-W. Cheong, *Appl. Phys. Lett.*, 2009, **95**, 092506.
- 19 X. Moya, *et al.*, *Nat. Mater.*, 2013, **12**, 52.
- 20 M. Phan, S. Chandra, N. Bingham, H. Srikanth, C. Zhang, S. Cheong, T. Hoang and H. Chinh, *Appl. Phys. Lett.*, 2010, **97**, 242506.
- 21 M. Phan, M. Morales, N. Bingham, H. Srikanth, C. Zhang and S. Cheong, *Phys. Rev. B: Condens. Matter Mater. Phys.*, 2010, **81**, 094413.
- 22 S. Xu, Q. Shi, J. Ju, Z. Han, B. Qian, D. Wang, P. Zhang, X. Jiang and Y. Du, *J. Nanosci. Nanotechnol.*, 2016, **16**, 2042.
- 23 T. Zhang, T. Zhou, T. Qian and X. Li, *Phys. Rev. B: Condens. Matter Mater. Phys.*, 2007, **76**, 174415.
- 24 D. D. Belyea, T. S. Santos and C. W. Miller, *J. Appl. Phys.*, 2012, **111**, 07A935.
- 25 T. Mukherjee, S. Sahoo, R. Skomski, D. J. Sellmyer and C. Binek, *Phys. Rev. B: Condens. Matter Mater. Phys.*, 2009, **79**, 144406.
- 26 S. Thota, Q. Zhang, F. Guillou, U. Lüders, N. Barrier, W. Prellier, A. Wahl and P. Padhan, *Appl. Phys. Lett.*, 2010, **97**, 112506.
- 27 K. Du, *et al.*, *Nat. Commun.*, 2015, **6**, 6179.
- 28 M. Uehara, S. Mori, C. H. Chen and S. W. Cheong, *Nature*, 1999, **399**, 560.
- 29 W. Wu, C. Israel, N. Hur, S. Park, S. W. Cheong and A. de Lozanne, *Nat. Mater.*, 2006, **5**, 881.
- 30 K. Zhang, *et al.*, *Proc. Natl. Acad. Sci. U. S. A.*, 2015, **112**, 9558.
- 31 L. Zhang, C. Israel, A. Biswas, R. L. Greene and L. A. De, *Science*, 2002, **298**, 805.
- 32 Y. Zhu, *et al.*, *Nat. Commun.*, 2016, **7**, 11260.
- 33 B. G. Shen, J. R. Sun, F. X. Hu, H. W. Zhang and Z. H. Cheng, *Adv. Mater.*, 2009, **21**, 4545.